Pergamon

PII: S0301-9322(96)00043-2

Int. J. Multiphase Flow Vol. 22, No. 6, pp. 1223–1246, 1996

0301-9322/96 $15.00 + 0.00

STEADY SUSPENSION FLOWS INTO TWO-DIMENSIONAL HORIZONTAL AND INCLINED CHANNELS

I. MISKIN[1], L. ELLIOTT[1], D. B. INGHAM[1] and P. S. HAMMOND[2]

[1]Department of Applied Mathematical Studies, University of Leeds, Leeds LS2 9JT, U.K.
[2]Schlumberger Cambridge Research Limited, P.O. Box 153, Cambridge CB3 0HG, U.K.

(Received 7 April 1996; in revised form 12 June 1996)

Abstract—In this study a model which was developed previously is used to theoretically investigate the steady flow of a particulate suspension into two-dimensional horizontal and inclined channels. The continuity equation for the fluid and the simplified two-dimensional Navier–Stokes equations are then solved together with a particle concentration equation. This latter equation is formulated by considering the balance between the particle flux due to gravity with the corresponding particle fluxes due to convection and shear-induced diffusion. The resulting coupled system of equations is solved numerically using a specialised finite-difference method. It is found, for the parameter range for flows of proppants in hydraulic fractures, that when the suspension enters the channel with a uniform velocity profile it almost instantaneously becomes parabolic. In addition, the effects of particle sedimentation are most dominant in the entrance region, but further downstream such effects are balanced as shear-induced particle diffusion becomes more important. It is also shown that the suspension flow depends critically on the choice of the parameters used, e.g. the ratio of the particle radius to the height of the channel. Copyright © 1996 Elsevier Science Ltd.

Key Words: suspension flows, shear-induced diffusion

1. INTRODUCTION

It has been reported in earlier studies, e.g. Leighton & Acrivos (1986, 1987) and Phillips *et al.* (1992), that, within particulate suspensions which undergo shear, a flux of particles is induced from regions of high to low shear and from regions of high to low particle concentration. This phenomena, known as shear-induced diffusion or migration, is caused by irreversible hydrodynamic interactions between neighbouring particles and it is found to be different from conventional Brownian diffusion which arises from molecular motion.

Shear-induced migration is of great importance in many industrial applications, including the manufacture of composite materials, the separation of particulates from slurries and the safe production of solid rocket fuels. This phenomena also influences the process of proppant placement within hydraulic fractures which are used in the hydrocarbon extraction industry. In this type of operation proppant particles, which are transported within a carrier fluid that is pumped into the fracture, are required to sediment evenly along the length of the fracture and thus keep it wedged open. However, occasionally proppant particles sediment with a high settling velocity and this may result in the formation of proppant banks at the bottom of the fracture. As a result, a bridge could form across the fracture and prevent the deep penetration of particles which may lead to fracture closure. A low settling velocity results in a more even distribution of proppant particles along the entire length of the fracture and thus can avert fracture closure. Shear-induced migration is one aspect which is thought to interfere with the settling rates of proppant particles and if properly exploited it may have a positive influence on the process of proppant placement within hydraulic fractures.

There are many different types of interparticle interactions that may be of importance within concentrated suspension flows. Since a model which rigorously takes into account each of these effects for a many particle system would be computationally expensive, especially in view of the fact that industrially interesting flows are generally complex in nature, a simpler model which takes into account the relevant physics of a suspension must be devised. Hence, a continuum model, along the lines of that considered by Leighton & Acrivos (1986), must be used. In such a model empirical expressions are formulated for each of the particle fluxes resulting from the key

mechanisms occurring within the suspension and a concentration equation is then developed by considering simple balances between the various particle fluxes. In the studies undertaken by Leighton & Acrivos (1986) and Schaflinger *et al.* (1990) the fully-developed Couette and Poiseuille shear flows within rectangular channels, respectively, were among the flows examined. In these studies the conservation of mass and the one-dimensional momentum equation were solved, together with the particle concentration equation, which was developed by considering a balance between the downward flux of particles due to sedimentation and the upward flux due to shear-induced diffusion. Later, Zhang & Acrivos (1994) used a similar model to theoretically examine a more intricate fully-developed suspension flow within a horizontal pipe. More recently, Pelekasis & Acrivos (1995) considered the problem of a steady laminar flow of a well-mixed suspension being convected steadily past a horizontal flat plate. They found that the particle concentration took the uniform upstream value everywhere except in two layers either side of the plate due to the presence of shear-induced particle diffusion balancing the particle flux due to convection and sedimentation.

In the present study we consider the steady laminar plug flow a well-mixed suspension which enters a rectangular channel as this is a reasonable model for the flow of proppant particles entering a hydraulic fracture. It should be noted that if dynamic effects are not present then three distinct regions exist, namely, a sediment layer near the bottom surface, the initial suspension in the middle and a clear fluid layer near the top surface of the channel, and each of these regions is separated by kinematic shocks. The structure of the concentration within the sedimentation layer depends upon both the initial concentration and the assumed form of the hindered settling function. However, with the inclusion of convection and diffusion effects only a clear fluid region and a continuously varying suspension layer exist. Within the channel the governing non-dimensional particle concentration equation, which takes into account the effects of convection, diffusion and sedimentation, and the two-dimensional momentum equations are simplified by considering the magnitude of each of the terms present when values of the important parameters relating to the flow entering a hydraulic fracture are utilized. The strongly coupled governing nonlinear system of equations is then solved by devising a specialised numerical scheme and the results discussed.

2. FORMULATION

Suppose a suspension of particles is driven by a pressure gradient into a 2-dimensional channel of height H which is inclined at an angle α to the horizontal, see figure 1. A Cartesian coordinate system is set up such that the x^* and z^*-coordinates are along and perpendicular to the bottom

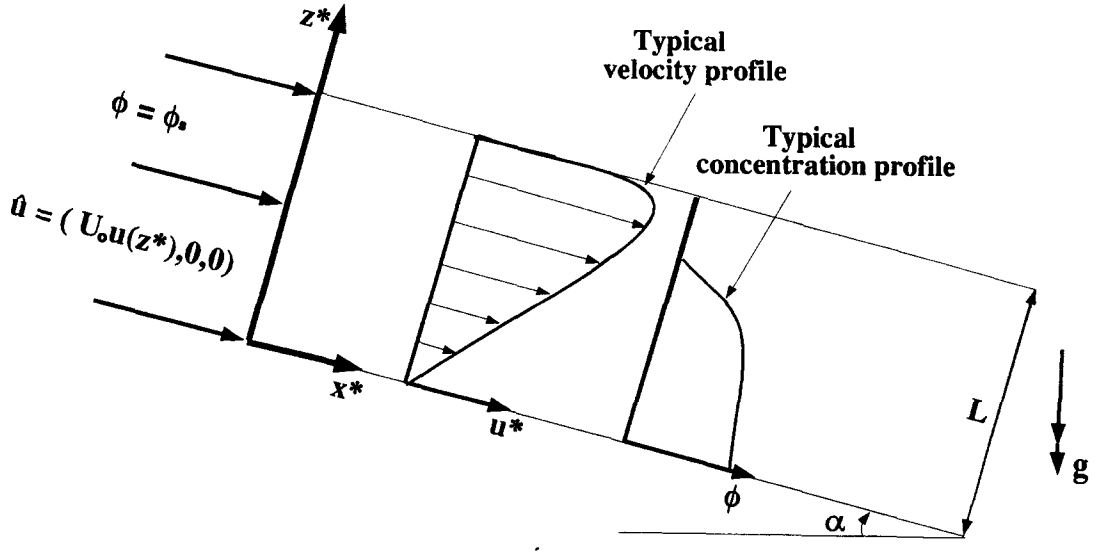

Figure 1. Schematic diagram of the coordinate system, notation and typical velocity and concentration profiles.

surface of the channel, respectively, and $x^* = 0$ is at the entrance to the channel and the fluid velocity components are u^* and w^* in the x^* and z^*-directions, respectively, i.e. $\underline{u}^* = (u^*, 0, w^*)$. It should be noted that the superscript * denotes dimensional quantities throughout. The suspension is assumed to enter the channel with a x^*-component of velocity $u^* = U_0\hat{u}(z^*)$ and with an initial concentration ϕ_s, where U_0 is the characteristic fluid velocity in the x^*-direction and $\hat{u}$ is a dimensionless function. For mathematical simplicity the particles are assumed to be rigid spherical and of uniform size with a radius a, but an extension to other shaped particles is possible.

The obvious length scale in the z^*-direction is the height of the channel, H, and suppose the fluid velocity scale in the x^*-direction is U_0. The corresponding dimensional scales for the length in the x^*-direction and the velocity in the z^*-direction are taken to be βH and σU_0, respectively, where σ and β are parameters to be determined. It should be noted that the velocity scale in the z^*-direction can be taken to be the Stokes velocity, u_t, i.e. the terminal velocity at which a single particle falls through a clear fluid, and this is given by

$$u_t = \frac{2}{9}\frac{ga^2(\rho_2 - \rho_1)}{\mu_1} \qquad [1]$$

for a rigid sphere of radius a and density ρ_2 which moves through a fluid of density ρ_1 and viscosity μ_1. Thus, the dimensionless variables are given by

$$x = \frac{x^*}{(\beta H)}, \quad z = \frac{z^*}{H}, \quad u = \frac{u^*}{U_0}, \quad w = \frac{w^*}{(\sigma U_0)} = \frac{w^*}{u_t}, \quad p = \frac{p^*}{(\rho_1 U_0^2)}, \quad \rho_r = \frac{\rho^*}{\rho_1}, \quad \mu_r = \frac{\mu^*}{\mu_1} \qquad [2]$$

where p is the dimensionless pressure field, ρ_r and μ_r are the relative density and viscosity between the particulate suspension and the clear fluid, respectively, and are expressed as

$$\rho_r = \frac{\rho^*}{\rho_1} = (1 + \epsilon\phi) \quad \text{with} \quad \epsilon = \frac{\rho_2 - \rho_1}{\rho_1} \geqslant 0 \qquad [3]$$

and

$$u_r = \frac{u^*}{\mu_1} = \left[1 + \frac{1.5\phi}{1 - \dfrac{\phi}{\phi_0}}\right]^2, \qquad [4]$$

respectively, see Zhang & Acrivos (1994), where ϕ is the local particle volume fraction and ϕ_0 is the volume fraction of particles in the state of close packing and typically takes the value 0.58, see Leighton & Acrivos (1996).

For an incompressible flow, assuming that the suspension can be considered as an effective continuum and that its rheology is Newtonian, the dimensionless continuity equation takes the form

$$\frac{1}{\sigma\beta}\frac{\partial u}{\partial x} + \frac{\partial w}{\partial z} = 0. \qquad [5]$$

As both the terms in [5] should balance we therefore take $\sigma\beta = 1$, i.e.

$$\frac{\partial u}{\partial x} + \frac{\partial w}{\partial z} = 0 \qquad [6]$$

and from [2] we have the relation

$$\beta = \frac{1}{\sigma} = \frac{U_0}{u_t}. \qquad [7]$$

For steady flow, the particle mass balance is

$$\nabla^* \cdot (\underline{u}^*\phi) = -\nabla^* \cdot \underline{J} \qquad [8]$$

where $\underline{J}$ is a combination between the diffusive flux due to shear-induced migration, $\underline{N}_s$, and the sedimentation flux due to gravity, $\underline{N}_g$, which is given by

$$\underline{J} = \underline{N}_s + \underline{N}_g. \quad [9]$$

By using simple scaling arguments, Phillips *et al.* (1992) derived an expression for the flux resulting from shear-induced diffusion, which was given as

$$\underline{N}_s = -D_c \nabla^* \phi - D_s \nabla^* \dot{\gamma}^* \quad [10]$$

where the dimensional absolute shear rate, $\dot{\gamma}^*$, is expressed as

$$\dot{\gamma}^* = \frac{du^*}{dz^*} \quad [11]$$

and D_c and D_s are both dimensional diffusion coefficients whose dimensionless forms are

$$\hat{D}_c \equiv \frac{D_c}{a^2 \dot{\gamma}^*} = K_c \phi + K_\mu \phi^2 \frac{1}{\mu_r} \frac{d\mu_r}{d\phi} \quad [12]$$

and

$$\hat{D}_s \equiv \frac{D_s}{a^2} = K_c \phi^2 \quad [13]$$

where K_c and K_μ are constants which have to be determined experimentally. For all our calculations we will impose K_c and K_μ to be 0.43 and 0.65, respectively, i.e. the values obtained in Phillips *et al.* (1992). The expression for the sedimentation flux is given by

$$\underline{N}_g = \underline{u}_s \phi \quad [14]$$

where $\underline{u}_s$ is the relative velocity of the particles with respect to the bulk flow and it is given by

$$\underline{u}_s = u_t f(\phi)(\underline{g}/g) \quad [15]$$

$$= \underline{u}_p - \underline{u}^* \quad [16]$$

where $\underline{u}_p$ is the particle velocity. The hindered settling function, $f(\phi)$, is expressed by Leighton & Acrivos (1986) as

$$f(\phi) = \frac{1 - \phi}{\mu_r}. \quad [17]$$

By applying the continuity [6] to [8], and neglecting the effects of gradients in the shear in [10], the dimensionless form of the particle concentration equation can be written as

$$u \frac{\partial \phi}{\partial x} + w \frac{\partial \phi}{\partial z} = \lambda^2 \left[\frac{1}{\beta} \frac{\partial}{\partial x} \left(\frac{\partial u}{\partial z} \hat{D}_c(\phi) \frac{\partial \phi}{\partial x} \right) + \beta \frac{\partial}{\partial z} \left(\frac{\partial u}{\partial z} \hat{D}_c(\phi) \frac{\partial \phi}{\partial z} \right) \right] + \frac{\partial (\phi f)}{\partial z} \cos \alpha. \quad [18]$$

The effects of gradients in shear are neglected since, in this case, shear-induced diffusion due to a gradient of concentration dominates, see Schaflinger *et al.* (1995), however, they may be significant for flows within horizontal pipes, see Zhang & Acrivos (1994). Additionally, their inclusion would result in third-order spatial derivatives occurring in some of the velocity terms appearing in the governing particle concentration equation which would make the problem much more difficult to solve. The dimensionless x and z-momentum equations are given by

$$u \frac{\partial u}{\partial x} + w \frac{\partial u}{\partial z} + \frac{1}{\rho_r(\phi)} \frac{\partial p}{\partial x} = \frac{1}{\rho_r(\phi)} \frac{\lambda}{\beta \mathrm{Rp}} \left[\frac{1}{\beta} \frac{\partial}{\partial x} \left(\mu_r(\phi) \frac{\partial u}{\partial x} \right) + \beta \frac{\partial}{\partial z} \left(\mu_r(\phi) \frac{\partial u}{\partial z} \right) \right]$$

$$+ \frac{1}{\rho_r(\phi)} \left(\frac{9}{2\lambda \beta \mathrm{Rp}} \right) \phi \sin \alpha \quad [19]$$

and

$$u\frac{\partial w}{\partial x}+w\frac{\partial w}{\partial z}+\frac{\beta^2}{\rho_r(\phi)}\frac{\partial p}{\partial z}=\frac{1}{\rho_r(\phi)}\frac{\lambda}{\beta \mathrm{Rp}}\left[\frac{1}{\beta}\frac{\partial}{\partial x}\left(\mu_r(\phi)\frac{\partial w}{\partial x}\right)+\beta\frac{\partial}{\partial z}\left(\mu_r(\phi)\frac{\partial w}{\partial z}\right)\right]$$

$$-\frac{1}{\rho_r(\phi)}\left(\frac{9}{2\lambda \mathrm{Rp}}\right)\phi\cos\alpha \quad [20]$$

respectively, where

$$\lambda=\frac{a}{H}, \quad [21]$$

and the dimensionless quantity Rp is the particle Reynolds number which is given by

$$\mathrm{Rp}=\frac{\rho_1 u_t a}{\mu_1}. \quad [22]$$

A knowledge of the range of values taken by the parameters in [18]–[20] is required if we are to be able to model a particular process involving the flow of a suspension in a rectangular channel. For the case of a hydraulic fracture this is found by considering a typical range of field variables, see for example Economides & Nolte (1989), namely $\beta \sim O(10)$ to $O(10^3)$ and $\lambda \sim O(10^{-3})$ to $O(10^{-1})$. Additionally, it is well known that the effects of shear-induced diffusion are usually observed when the particle Reynolds number, Rp, is $O(10^{-3})$ or less, see Leighton & Acrivos (1987). Although Rp falls well within this domain, in order to limit the number of parameters occurring in our problem the value of the particle Reynolds number is imposed at 10^{-3} and further ϵ is taken to be unity.

In the present analysis the three non-dimensional parameters governing the shear-induced diffusion are λ, Rp and β, whereas Pelekasis & Acrivos (1995) opted for E, Re and Gr, where $E=\lambda(H/L)$, $\mathrm{Re}=L\beta\mathrm{Rp}/(\lambda H)$, $\mathrm{Gr}=L^3\mathrm{Rp}/(\lambda H)^3$ with L a function of Re, Gr and E. However, if we retain their choice of parameters in the physical situation being considered here we would be faced either with increasing the number of non-dimensional parameters by introducing the extra parameter H/L or, since H is a naturally occurring length scale, replacing the artificially introduced length scale L by H. In a hydraulic fracture the ranges of the alternative non-dimensional parameters E, Re and Gr would be $O(10^{-3})$ to $O(10^{-1})$, $O(1)$ to $O(10^3)$ and $O(10)$ to $O(10^5)$, respectively. The advantages of the dimensionless groups chosen by Pelekasis & Acrivos (1995), assuming L is replaced by H so that $E=\lambda$ and the number of non-dimensional parameters remains the same, are

(i) it avoids combinations of large and small parameters, e.g. $E\mathrm{Re}$, $E\mathrm{Gr}$, arising in the governing equations,

(ii) it allows the experimentalist to easily alter each individual non-dimensional parameter, i.e. change E by varying the radius of the particles, change Re by varying the characteristic fluid velocity and change Gr by varying the density of the particles.

Unfortunately, the present choice of non-dimensional parameters, namely, λ, Rp and β fails to satisfy the first criterion since combinations such as $\lambda^2\beta$ and $\lambda\beta\mathrm{Rp}$ are present in [23] and [24] and the second criterion is only met in the case of β, since it is possible to change only this quantity by varying the characteristic fluid velocity. Changes to only λ would require modifications to the experimental apparatus in the form of adjustments to H, whilst changes to Rp would require complex adjustments to both the characteristic fluid velocity and to the fluid and particle parameters. However, it should be emphasized that the physical problem under consideration is that of shear-induced diffusion within a fracture where conditions correspond to a small fixed value of Rp, taken as 10^{-3} in *all* our calculations, and we wish to investigate the effects of changes to both the characteristic fluid velocity and to the fracture width. Whilst the former change can be achieved using either group of non-dimensional quantities, the latter one is only possible with the present set, since changes to the fracture width affect Re and Gr as well as λ.

In [18] and [19] it is clear that the term which includes a factor $1/\beta$ is substantially smaller in magnitude than the term which has a factor β. Hence, for a hydraulic fracture [18] and [19] can be approximated by

$$u\frac{\partial\phi}{\partial x}+w\frac{\partial\phi}{\partial z}=\lambda^2\beta\frac{\partial}{\partial z}\left(\frac{\partial u}{\partial z}\hat{D}_c(\phi)\frac{\partial\phi}{\partial z}\right)+\frac{\partial(\phi f(\phi))}{\partial z}\cos\alpha \qquad [23]$$

$$u\frac{\partial_u}{\partial x}+w\frac{\partial u}{\partial z}+\frac{1}{\rho_r(\phi)}\frac{\partial p}{\partial x}=\frac{\lambda}{\rho_r(\phi)\mathrm{Rp}}\frac{\partial}{\partial z}\left(\mu_r(\phi)\frac{\partial u}{\partial z}\right)+\frac{1}{\rho_r(\phi)}\left(\frac{9}{2\lambda\beta\mathrm{Rp}}\right)\phi\sin\alpha. \qquad [24]$$

In [20] the terms involving β^2 and $1/(\lambda\mathrm{Rp})$ are dominant in the case of a hydraulic fracture and therefore we have

$$\frac{\partial p}{\partial z}=-\left(\frac{9}{2\lambda\beta^2\mathrm{Rp}}\right)\phi\cos\alpha. \qquad [25]$$

To complete the formulation we need to consider the boundary and entrance conditions. Although there is evidence of particle slip along solid walls in suspension flows, see Yilmazer & Kalyon (1989), it was shown by Schaflinger *et al.* (1990) that this had very little effect on the solutions obtained for a fully-developed Hagen–Poiseuille flow in a horizontal channel. Hence, in this study the condition of no-slip is assumed at both solid boundaries. Additionally, at the boundaries there is no net flux of fluid, $\underline{u}\cdot\underline{n}$, or particles $\underline{J}\cdot\underline{n}$, where $\underline{n}$ is a normal vector to the boundaries, and at the entrance to the channel the velocity is $(U_0\hat{u}(z^*), 0, 0)$ and the particle concentration is ϕ_s. The dimensionless boundary and entrance conditions are given by:

$$\text{At}\quad z=0,\quad 0<x<\infty: u=w=0\quad\text{and}\quad \lambda^2\beta\hat{D}_c\frac{\partial u}{\partial z}\frac{\partial\phi}{\partial z}+\phi f\cos\alpha=0 \qquad [26]$$

$$\text{At}\quad z=1,\quad 0<x<\infty: u=w=0\quad\text{and}\quad \lambda^2\beta\hat{D}_c\frac{\partial u}{\partial z}\frac{\partial\phi}{\partial z}+\phi f\cos\alpha=0 \qquad [27]$$

$$\text{At}\quad x=0,\quad 0\leqslant z\leqslant 1: u=\hat{u}(z),\quad w=0\quad\text{and}\quad \phi=\phi_s \qquad [28]$$

where $\hat{u}(z)$ and ϕ_s are to be specified and in the case of plug flow $\hat{u}(z)=$ constant.

[It should be noted that the boundary and entrance conditions [26]–[28] are not affected by the simplifications made because we are considering parameters in the range appropriate to a hydraulic fracture.] Equations [6] and [23]–[25] and the boundary conditions [26]–[28] represent a coupled set of non-linear, parabolic partial differential equations which can be solved numerically using a marching procedure and solving the resulting algebraic equations iteratively at each x location before proceeding along the fracture. Since we know that far from the entrance to the channel sharp gradients in concentration may occur, obtaining a convergent solution is likely to cause a problem. To overcome this possible difficulty we may be required to use a nonlinear grid, or an adaptive grid system, which becomes finer in regions where the solution varies most rapidly and coarser in regions where there is little variation in the unknown variables.

It should be noted that if the plug flow becomes fully-developed then there is no x-dependence and it can be deduced from [6] and [23]–[28] that

$$\lambda^2\beta\frac{\mathrm{d}u}{\mathrm{d}z}\hat{D}_c\frac{\mathrm{d}\phi}{\mathrm{d}z}+\phi f\cos\alpha=0 \qquad [29]$$

and

$$\frac{\mathrm{d}}{\mathrm{d}z}\left(\mu_r\frac{\mathrm{d}u}{\mathrm{d}z}\right)=-K-\left(\frac{9}{2\lambda^2\beta}\right)\phi\sin\alpha \qquad [30]$$

where K is a constant. The parameters λ and β can be used to obtain the modified Shields number, κ, see Schaflinger *et al.* (1990), and it is given by

$$\kappa = \lambda^2\beta \int_0^1 (1 - \phi_s)\hat{u}(z)\,\mathrm{d}z. \qquad [31]$$

Therefore, provided the same parameter values are used, the initial two-dimensional plug flow will eventually tend after a non-dimensional development length, L_ϕ/H, down the channel to a fully-developed flow situation which is the same as the solutions obtained via [29] and [30]. The criterion given by Schaflinger *et al.* (1995) is

$$\frac{L_\phi}{H} \sim \frac{\kappa H^2}{8a^2} \qquad [32]$$

which becomes, on using [31],

$$\frac{L_\phi}{H} \sim \frac{\beta}{8} \int_0^1 (1 - \phi_s)\hat{u}(z)\,\mathrm{d}z. \qquad [33]$$

3. NUMERICAL PROCEDURE

In order to obtain the particle concentration and fluid velocity profiles throughout the channel the coupled continuity, concentration, x-momentum and z-momentum equations, namely [6] and [23]–[25], respectively, must be solved subject to the boundary and entrance conditions [26]–[28].

The continuity [6] is automatically satisfied by introducing the non-dimensional stream-function, ψ, in the usual manner, namely,

$$u = \frac{\partial\psi}{\partial z} \quad \text{and} \quad w = -\frac{\partial\psi}{\partial x}. \qquad [34]$$

The streamfunction formulation [34] will result in third-order derivatives in ψ arising in [23] and [24]. To reduce the order of such derivatives we let

$$s(x, z) = \frac{\partial\psi}{\partial z} \qquad [35]$$

and

$$s_1 = s(x, z), \quad s_2 = s(x + \delta x, z), \quad \phi_1 = \phi(x, z), \quad \phi_2 = (x + \delta x, z) \qquad [36]$$

where δx is a small step length in the x-direction. Further, we write

$$S = s_1 + s_2, \quad \Phi = \phi_1 + \phi_2 \quad \text{and} \quad s \approx \tfrac{1}{2}S, \quad \phi \approx \tfrac{1}{2}\Phi. \qquad [37]$$

On substitution of relations [34]–[37] into [23] we obtain

$$4S\left(\frac{\Phi - 2\phi_1}{\delta x}\right) - 4\left(\int_0^z \frac{S - 2s_1}{\delta x}\,\mathrm{d}z\right)\frac{\partial\Phi}{\partial z} = 4E(\tfrac{1}{2}\Phi)\frac{\partial\Phi}{\partial z}$$

$$+ \lambda^2\beta\left[2\hat{D}_c(\tfrac{1}{2}\Phi)\left\{\frac{\partial^2 S}{\partial z^2}\frac{\partial\Phi}{\partial z} + \frac{\partial S}{\partial z}\frac{\partial^2\Phi}{\partial z^2}\right\} + \hat{D}_c'(\tfrac{1}{2}\Phi)\frac{\partial S}{\partial z}\left(\frac{\partial\Phi}{\partial z}\right)^2\right] \qquad [38]$$

and [24] has been combined with the integral form of [25] to become

$$2S\left(\frac{S-2s_1}{\delta x}\right)+\frac{4}{\rho_r(\frac{1}{2}\Phi)}\left\{-\left(\frac{9\cos\alpha}{2\lambda\beta^2\mathrm{Rp}}\right)\int_0^z\frac{\Phi-2\phi_1}{\delta x}\,\mathrm{d}z+\frac{\mathrm{d}p_0}{\mathrm{d}x}\right\}-2\left(\int_0^z\frac{S-2s_1}{\delta x}\,\mathrm{d}z\right)\frac{\partial S}{\partial z}$$

$$=\frac{1}{\rho_r(\frac{1}{2}\Phi)}\frac{\lambda}{\mathrm{Rp}}\left\{2\mu_r(\tfrac{1}{2}\Phi)\frac{\partial^2 S}{\partial z^2}+\mu_r'(\tfrac{1}{2}\Phi)\frac{\partial S}{\partial z}\frac{\partial\Phi}{\partial z}\right\}+\frac{1}{\rho_r(\frac{1}{2}\Phi)}\left(\frac{9\sin\alpha}{\lambda\beta\mathrm{Rp}}\right)\Phi \quad [39]$$

where $p_0(x)=p(x,0)$ and

$$E(\phi)=\left[\frac{1-2\phi}{\mu_r(\phi)}-\frac{\phi(1-\phi)}{\mu_r^2(\phi)}\mu_r'(\phi)\right]\cos\alpha. \quad [40]$$

The boundary conditions [26]–[28] become

$$S=0 \quad \text{and} \quad \hat{D}_c\frac{\partial S}{\partial z}\frac{\partial\Phi}{\partial z}+\frac{2}{\lambda^2\beta}\Phi f(\tfrac{1}{2}\Phi)\cos\alpha=0 \quad \text{at} \quad z=0;\quad 0<x<\infty \quad [41]$$

$$S=\int_0^z\frac{S-2s_1}{\delta x}\,\mathrm{d}z=0 \quad \text{and} \quad \hat{D}_c\frac{\partial S}{\partial z}\frac{\partial\Phi}{\partial z}+\frac{2}{\lambda^2\beta}\Phi f(\tfrac{1}{2}\Phi)\cos\alpha=0 \quad \text{at} \quad z=1;\quad 0<x<\infty \quad [42]$$

and

$$s_1(x,z)=\hat{u}(z) \quad \text{and} \quad \phi_1(x,z)=\phi_s \quad \text{at} \quad x=0;\quad 0\leqslant z\leqslant 1. \quad [43]$$

It is expected that the unknown variables, especially the concentration, will change rapidly in the neighbourhood of the suspension-clear fluid interface. In order to resolve these rapid variations in the unknown variable it is necessary to have a sufficiently large number of finite-difference grid points across the channel but this leads to larger CPU times being required for the numerical calculations to converge. In order to reduce the CPU time it is necessary to use a non-uniform distribution of grid points so that the spacing between the points becomes smaller in regions where the unknown variables change rapidly and larger elsewhere.

A finite-difference scheme for a non-uniform grid system is derived as follows. Suppose Θ is a continuous function with continuous derivatives and that $\{z_n\}\in[0,1]$ is a monotonically increasing sequence. By using Taylor series, and neglecting terms which are $O(\Delta z_1)^4$, $O(\Delta z_2)^4$, we obtain

$$\Theta(z_j+\Delta z_1)=\Theta(z_j)+(\Delta z_1)\Theta'(z_j)+\tfrac{1}{2}(\Delta z_1)^2\Theta''(z_j)+\tfrac{1}{6}(\Delta z_1)^3\Theta'''(z_j)+\cdots \quad [44]$$

and

$$\Theta(z_j+\Delta z_2)=\Theta(z_j)-(\Delta z_2)\Theta'(z_j)+\tfrac{1}{2}(\Delta z_2)^2\Theta''(z_j)-\tfrac{1}{6}(\Delta z_2)^3\Theta'''(z_j)+\cdots \quad [45]$$

where

$$\Delta z_1=z_{j+1}-z_j \quad [46]$$

and

$$\Delta z_2=z_j-z_{j-1}. \quad [47]$$

By subtracting [45] from [44], and neglecting terms which are $O(\Delta z_1)^3$, $O(\Delta z_2)^3$, we obtain

$$\Theta(z_j+\Delta z_1)-\Theta(z_j-\Delta z_2)=(\Delta z_1+\Delta z_2)\Theta'(z_j)+\tfrac{1}{2}((\Delta z_1)^2-(\Delta z_2)^2)\Theta'''(z_j)+\cdots \quad [48]$$

which on simplification, via [46] and [47], becomes

$$\Theta'(z_j)=\frac{\Theta(z_{j+1})-\Theta(z_{j-1})}{z_{j+1}-z_{j-1}}+O(\Delta z_1-\Delta z_2). \quad [49]$$

Now, by multiplying [44] and [45] by Δz_2 and Δz_1, respectively, and adding we obtain

$$(\Delta z_2)\Theta(z_j + \Delta z_1) + (\Delta z_1)\Theta(z_j - \Delta z_2) = (\Delta z_2 + \Delta z_1)\Theta(z_j) + \tfrac{1}{2}(\Delta z_1)(\Delta z_2)(\Delta z_2 + \Delta z_1)\Theta''(z_j) + \tfrac{1}{6}(\Delta z_2)((\Delta z_1)^2 - (\Delta z_2)^2)\Theta'''(z_j) \quad [50]$$

which on simplification, via [46] and [47], becomes

$$\Theta''(z_j) = \frac{2}{z_{j+1} - z_{j-1}}\left[\left\{\frac{\Theta(z_{j+1}) - \Theta(z_j)}{z_{j+1}z_j}\right\} - \left\{\frac{\Theta(z_j) - \Theta(z_{j-1})}{z_j - z_{j-1}}\right\}\right] + O(\Delta z_1 - \Delta z_2). \quad [51]$$

It should be noted that the finite-difference relations [49] and [51] are both first-order unless $\Delta z_1 = \Delta z_2$ and in which case they become second-order. For this reason the rate of non-uniformity of the grid distribution must be kept small in regions where greater accuracy is required.
Let

$$z_j = P(w_j) \quad [52]$$

where P is a monotonically increasing polynomial function and

$$w_j = (j - 1)/N \quad [53]$$

where $N + 1$ is the total number of grid points across the channel. It should be noted that the polynomial function P is chosen so that $P(w_1) = P(0) \equiv 0$ and $P(w_{N+1}) = P(1) \equiv 1$.

By applying the finite-difference schemes, given by [49] and [51], to [38] and [40] we obtain

$$\begin{aligned}
&4(z_{j+1} - z_{j-1})^3 S_j(\Phi_j - 2\phi_{1,j}) - 4(z_{j+1} - z_{j-1})^2 I1_j(\Phi(_j + 1 - \Phi_{j-1}) \\
&= \delta x \lambda^2 \beta\Bigg[4\hat{D}_c(\tfrac{1}{2}\Phi_j)(z_{j+1} - z_{j-1})\left\{\left(\frac{S_{j+1} - S_j}{z_{j+1} - z_j} - \frac{S_j - S_{j-1}}{z_j - z_{j-1}}\right)(\Phi_{j+1} - \Phi_{j-1})\right. \\
&\left. + \left\{\frac{\Phi_{j+1} - \Phi_j}{z_{j+1} - z_j} - \frac{\Phi_j - \Phi_{j-1}}{z_j - z_{j-1}}\right)(S_{j+1} - S_{j-1})\right\} + \hat{D}_c'(\tfrac{1}{2}\Phi_j)(S_{j+1} - S_{j-1})(\Phi_{j+1} - \Phi_{j-1})^2\Bigg] \\
&+ 4\delta x(z_{j+1} - z_{j-1})^2 E(\tfrac{1}{2}\Phi_j)(\Phi_{j+1} - \Phi_{j-1})
\end{aligned} \quad [54]$$

and

$$\begin{aligned}
&2(z_{j+1} - z_{j-1})^2 S_j(S_j - 2s_{1,j}) - 2(z_{j+1} - z_{j-1}) I1_j(S_{j+1} - S_{j-1}) \\
&+ \frac{4(z_{j+1} - z_{j-1})^2}{\rho_r(\frac{1}{2}\Phi_j)}\left\{-\left(\frac{9\cos\alpha}{2\lambda\beta^2 \mathrm{Rp}}\right) I2_j + \frac{dp_0}{dx}\delta x - \left(\frac{9\sin\alpha}{4\lambda\beta \mathrm{Rp}}\right)\Phi_j \delta x\right\} \\
&= \frac{\delta x}{\rho_r(\frac{1}{2}\Phi_j)}\frac{\lambda}{\mathrm{Rp}}\left\{4(z_{j+1} - z_{j-1})\mu_r(\tfrac{1}{2}\Phi_j)\left(\frac{S_{j+1} - S_j}{z_{j+1} - z_j} - \frac{S_j - S_{j-1}}{z_j - z_{j-1}}\right)\right. \\
&\left. + \mu_r'(\tfrac{1}{2}\Phi_j)(S_{j+1} - S_{j-1})(\Phi_{j+1} - \Phi_{j-1})\right\},
\end{aligned} \quad [55]$$

respectively, where $j = 1, \ldots, N + 1$ and the boundary conditions [41] and [42] become

$$\hat{D}_c(\tfrac{1}{2}\Phi_1)\left\{\frac{(S_2 - S_0)(\Phi_2 - \Phi_0)}{4(z_2 - z_1)^2}\right\} + \frac{2}{\lambda^2\beta}\Phi_1 f(\tfrac{1}{2}\Phi_1)\cos\alpha = 0 \quad [56]$$

$$\hat{D}_c(\tfrac{1}{2}\Phi_{N+1})\left\{\frac{(S_{N+2} - S_N)(\Phi_{N+2} - \Phi_N)}{4(z_{N+1} - z_N)^2}\right\} + \frac{2}{\lambda^2\beta}\Phi_{N+1} f(\tfrac{1}{2}\Phi_{N+1})\cos\alpha = 0 \quad [57]$$

and

$$S_1 = S_{N+1} = 0, \quad I1_{N+1} = 0 \tag{58}$$

where the integral terms in [38] and [42] have been replaced by numerical approximations via the trapezoidal rule, i.e.

$$I1_1 = 0 \tag{59}$$

$$I1_j = I1_{j-1} + \tfrac{1}{2}\{(S_{j-1} - 2s_{1,j-1}) + (S_j - 2s_{1,j})\}(z_j - z_{j-1}) \tag{60}$$

$$I2_1 = 0 \tag{61}$$

$$I2_j = I2_{j-1} + \tfrac{1}{2}\{(\Phi_{j-1} - 2\phi_{1,j-1}) + (\Phi_j - 2\phi_{1,j})\}(z_j - z_{j-1}) \quad \text{for} \quad j = 2, N+1. \tag{62}$$

An iterative method is considered in order to solve the resulting nonlinear system of algebraic finite-difference [54]–[58]. This method entails the following steps:

(a) The initial solutions profiles for the velocity, $\hat{u}(z_j)$, and particle concentration, $\phi_s(z_j)$, are stored in the arrays $s_{1,j}$ and $\phi_{1,j}$, respectively. Approximate values for the quantities Φ_j are obtained via [37].

(b) At the next streamwise step, i.e. in the x-direction, the quantities S_j are calculated by solving the finite-difference version of the x-momentum [55] subject to the boundary conditions [58], with the values of $s_{1,j}$, $\phi_{1,j}$ and Φ_j, being substituted from (a). It should be noted that we solve $N+4$ equations with $N+4$ unknowns, namely, $(S_0, S_1, \ldots, S_{N+1}, S_{N+2})$ and $\mathrm{d}p_0/\mathrm{d}x$.

(c) The quantities Φ_j are calculated by solving the finite-difference version of the particle concentration [54], together with the corresponding boundary conditions [56] and [57], using the updated values of S_j obtained from step (b). In this case we solve $N+3$ equations with $N+3$ unknowns, namely, $(\Phi_0, \Phi_1, \ldots, \Phi_{N+1}, \Phi_{N+2})$.

(d) Steps (b) and (c) are then repeated using the updated values of S_j, Φ_j and $\mathrm{d}p_0/\mathrm{d}x$.

(e) This Newton iteration process is repeated until the difference between two consecutive solutions is less than some preassigned tolerance. In all the results presented in this work a value of 10^{-6} has been found to be sufficiently small in that any further reduction in this value produces results which are graphically indistinguishable from those presented. Typically convergence is achieved within about five iterations.

(f) The values of s_j and ϕ_j are calculated via the relations

$$s_j = S_j - s_{1,j}, \quad \Phi_j = \Phi_j - \Phi_{1,j} \quad \text{for} \quad j = 1, N+1 \tag{63}$$

and are stored in the arrays $s_{1,j}$ and $\phi_{1,j}$, respectively.

(g) We then march forwards to the next streamwise location and the steps (a)–(f) are repeated. The algorithm is repeated until two solutions at consecutive streamwise steps differ by less than 10^{-4}, where it is assumed that the fully-developed situation has been reached.

It should be noted that the solutions of the algebraic finite-difference equations were obtained using a hybrid method, see Powell (1970), which finds a zero of a system of N nonlinear functions N variables. The main advantage of this method is that the system of equations can be decoupled and thus the equation solver operates more efficiently. The step length in the x-direction was kept constant for most of our computations in order to maintain numerical stability.

Additionally, it should be noted that we obtained some solutions in which the particle concentration, ϕ, oscillated. In particular, this occurred in the region of the suspension-clear fluid interface which arose as a clear fluid layer formed below the top surface of the channel. In order to reduce such numerical noise in ϕ, we used a simple filtering procedure which consists of the following:

(A) If the computed value of ϕ is less than a preset constant, which is typically 10^{-3}, then we set $\phi \equiv 0$.

(B) If $\phi_k > \phi_{k-1}$, where the positive integer $k \in [2, N]$, i.e. if the particle concentration begins to increase with z in any region of the channel, then we impose

$$\phi_k \equiv \tfrac{1}{2}(\phi_{k-1} + \phi_{k+1}). \tag{64}$$

In the problem considered by Zhang & Acrivos (1994), similar numerical oscillations in the neighbourhood of the suspension-clear fluid interface were also encountered and in order to overcome these problems they used a simple filter procedure similar to that described in (A).

In order to check the computational accuracy of our simulations, we used the following test. At each streamwise locations, x, the particle flux must remain unchanged, i.e. we required

$$\int_0^1 \phi u \, dz = C \qquad [65]$$

where C is a constant. As a test problem the finite-difference equations [54]–[58] were solved with the starting velocity and concentration profiles imposed as $s_{1,j} = \hat{u}(z_j) = \frac{1}{6}$ and $\phi_{1,j} = \phi_s(z_j) = \frac{3}{20}$, respectively, which result in the constant C taking the value 2.5×10^{-2}. Additionally, the angle of inclination of the channel, α, was taken to be zero and the parameters λ and β were set to 0.05 and 50, respectively.

Initially, meshes with uniform grid spacings in the z-direction were employed. In this particular case errors in the magnitude of the particle flux, C, arose particularly for $x > O(10^{-1})$, i.e. when the particle concentration began to swell in the region below the suspension-clear fluid interface. For instance, even with 70 uniformly spaced grid points in the z-direction the error in the particle flux exceeded its required constant value by as much as 13%. By increasing the total number of grid points across the channel, i.e. reducing the grid spacings, it was found that obtaining a numerically stable solution in the neighbourhood of the suspension-clear fluid interface became increasingly difficult. In order to maintain numerical stability, i.e. prevent oscillations occurring in the solution in the region of the suspension-clear fluid interface, it was necessary to decrease the size of the step lengths taken in the x-direction, but this measure leads in turn to increased CPU times occurring. Even when the number of grid points was increased to 80, with the steplength in the x-direction decreased significantly from 10^{-4} to 10^{-5}, it was not possible to stop oscillations in the solution from occurring. Thus the solution procedure failed in the sense that a convergent solution to the finite-difference [54]–[58] could eventually no longer be attained. It should be noted that these oscillations could not be smoothed out by the simple filtering procedures (A) and (B) which were described earlier in this section.

To achieve a greater conservation in the magnitude of the particle flux it was necessary, when $x \gtrsim O(10^{-1})$, to increase the accuracy of the solution obtained in the region below the suspension-clear fluid interface. This was accomplished by using a mesh in the z-direction which had nonlinear grid spacings. By initially running the problem on a uniform coarse mesh in the z-direction it was possible to locate the region where the particle flux across the channel began to alter. Thus, by using this type of preconditioner, which did not require excessive CPU times, a suitable nonlinear mesh was constructed such that the errors in the particle flux could be reduced. In the nonlinear mesh used to solve the current problem, i.e. where λ and β were set at 0.05 and 50, respectively, each grid point in the mesh was obtained via the transformation relation

$$z_j = 2w_j^3 - 6\hat{z}w_j^2 + (6\hat{z} - 1)w_j \qquad [66]$$

where w_j is defined by [53] and $\hat{z} = 0.6$. It should be noted that $\hat{z}$ was chosen approximately, via the uniform coarse mesh calculations, as the suspension-clear fluid interface height when the flow became fully-developed. As mentioned earlier in this section, the rate of non-uniformity of the mesh affects the order of the numerical scheme used, i.e. the scheme becomes second-order in spatial accuracy if the rate of non-uniformity tends to be zero but it is reduced to first-order accuracy elsewhere. The mesh in the z-direction is finest in the 'critical' region close to the eventual suspension-clear fluid interface, i.e. in the neighbourhood of $z = 0.6$, and becomes coarser closer to the bottom and top surfaces of the channel, namely $z = 0$ and 1, respectively. Hence, the numerical scheme is second-order close to $z = 0.6$ but its accuracy reduces to first-order away from this region. The advantage of using this type of mesh is that numerical oscillations can be eliminated in the region of the moving suspension-clear fluid interface, whilst the behaviour of the solution in the critical region, in which errors can build in the particle flux, is predicted accurately without the need of excessive CPU times.

Table 1. The errors in the particle flux, when $\hat{u} = \frac{1}{6}$ and $\phi_s = \frac{3}{20}$ with $\mathrm{Rp} = 10^{-3}$, $\epsilon = 1$, $\lambda = 0.05$ and $\beta = 50$, as a function of the number of grid points when using either a uniform mesh or a non-uniform mesh created via [66] with $\hat{z} = 0.6$

Number of grid points	Maximum % error for uniform mesh	Maximum % error for non-uniform mesh
20	39	15
40	24	10
50	19	5
60	15	3
70	13	<1

Table 1 shows a comparison between the maximum percentage errors in the particle flux and the number of grid points in the z-direction for the non-uniform mesh which is given by the transformation [66]. It is observed that the errors in the particle flux reduce rapidly as the number of grid points in the z-direction increases. When 70 non-uniformly spaced grid points in the z-direction are used the percentage error in the magnitude of the particle flux drops to less than unity while when 70 uniformly spaced grid points were used the error is in excess of 13%.

4. RESULTS AND DISCUSSION

The finite-difference [54]–[58] were initially solved with the starting velocity and concentration profiles imposed as $s_{1,j} = \hat{u}(z_j) = \frac{1}{6}$ and $\phi_{1,j} = \phi_s(z_j) = \frac{3}{20}$, respectively, with the channel in a horizontal position, i.e. the angle of inclination, α, is zero. By using the iterative method, see section 3, it was possible to obtain convergent solutions to [54]–[58] and thus we were able to march forwards in the x-direction. Results have been produced for a wide variety of values of the parameters λ and β which correspond to the range of physical interest in experimental or hydraulic fracturing applications, see section 2. A typical sequence of results showing the evolution of the particle concentration and velocity profiles is illustrated in figure 2(a) and (b), respectively, where the parameters λ and β were set to typical values associated with the process of hydraulic fracturing, namely, 0.05 and 50, respectively, with $\hat{u} = \frac{1}{6}$ and $\phi_s = \frac{3}{20}$. The mesh system used to produce these accurate results is discussed in section 3.

From figure 2(a) it is observed that the particle concentration in the upper region of the channel depletes quite rapidly as we move in the x-direction. Even at $x = 0.01$ a layer of clear fluid of thickness about 0.05 is detected just below the upper boundary of the channel. In contrast, the particle concentration in the lower region of the channel increases markedly as we move in the x-direction. For instance, at $x = 0.01$ the particle concentration at the lower boundary of the channel is 0.38 compared to 0.15 at $x = 0$. The reason for these results is that the particle flux due to sedimentation dominates the diffusion effects at small values of x.

Eventually, the rate of depletion of the particle concentration in the upper region of the channel begins to decrease. This is illustrated in figure 2(a), where the height at which the suspension-clear fluid interface occurs does not change very significantly for the profiles at $x = 0.3$ and $x = 1.0$, i.e. it decreases by about 0.05 which is approximately the same decrease observed between $x = 0$ and $x = 0.01$. The reason for this is that the particle flux due to the shear-induced diffusion becomes more influential at larger values of x, since the shear rate within the suspension region begins to increase, and this counteracts the corresponding particle flux due to sedimentation more successfully than at smaller values of x. By combining figure 2(a) and (b), it can be seen that the rate of increase of the fluid velocity with respect to z, or the shear rate, begins to increase just below the suspension-clear fluid interface. Additionally, in figure 2(b) it is strikingly noticeable that the initially flat velocity profile nearly instantaneously becomes parabolic. The reason for the sudden transition between a flat and parabolic velocity profile can be seen by examining [24]. Since the parameter combination $\lambda/\mathrm{Rp} = 50$ in this case, the order of the viscous term in [24] is much larger than the corresponding inertial terms which are $O(1)$. Therefore, the velocity profile very rapidly becomes parabolic and this would be the eventual fully-developed result if no variations in ϕ occurred. However, since ϕ varies due to the effects of shear-induced diffusion and sedimentation, the u-component of velocity changes beyond the first step in the x-direction due to its coupling with ϕ occurring within the x-momentum equation [24].

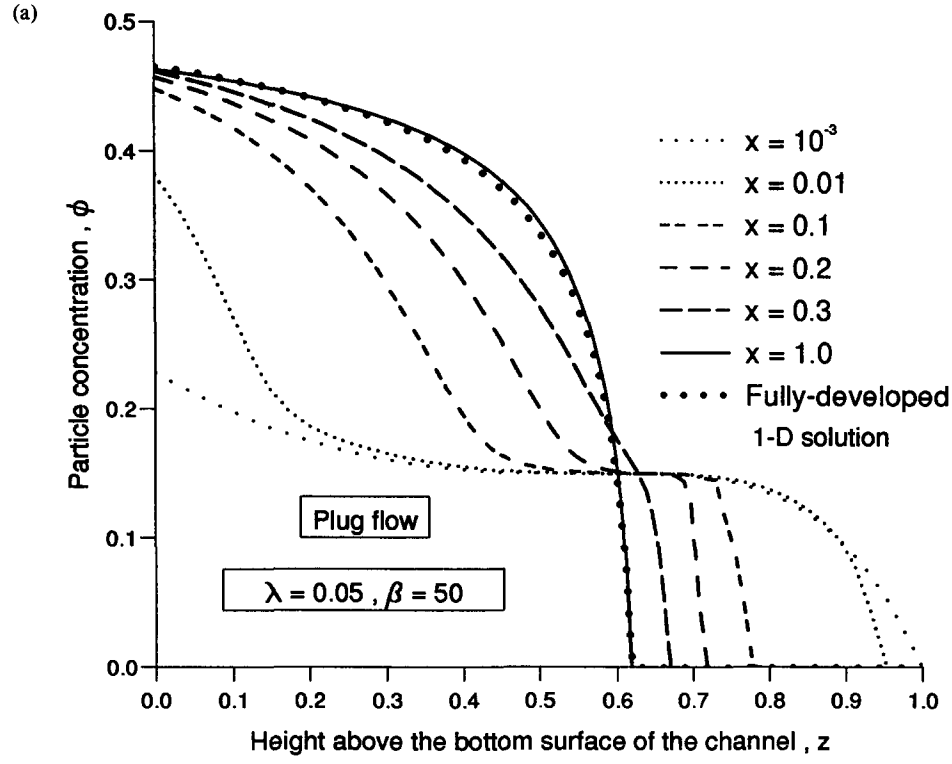

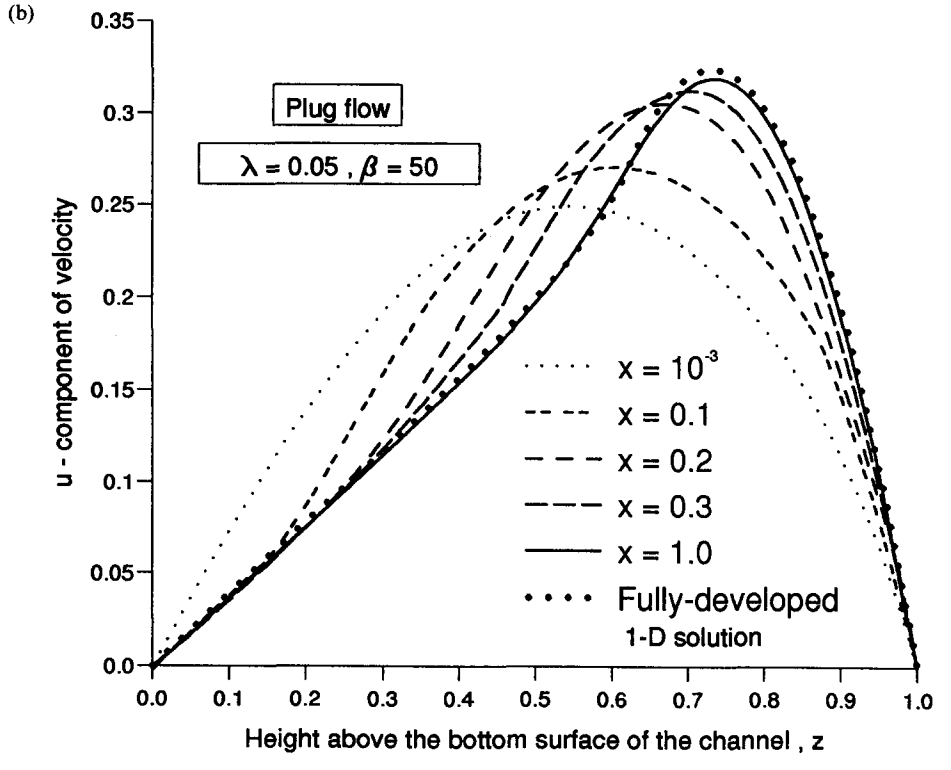

Figure 2. (a) The variation of the particle concentration, ϕ, with the height above the bottom surface of the channel, z, for an initial plug of well-mixed suspension of particle concentration 0.15 with $\mathrm{Rp} = 10^{-3}$, $\epsilon = 1$, $\lambda = 0.05$ and $\beta = 50$ flowing along a horizontal channel. (b) The variation of the u-component of velocity with the height above the bottom surface of the channel, z, with conditions as in (a).

It was shown in section 2 that as the flow becomes fully-developed the governing equations reduce to the one-dimensional Hagen–Poiseuille flow equations, namely, [29] and [30]. Thus, our particle concentration and velocity simulations should approach those for the corresponding one-dimensional fully-developed Hagen–Poiseuille problem. Figure 2(a) and (b) also show, for $\lambda = 0.05$ and $\beta = 50$, how the fully-developed concentration and velocity profiles, respectively, compare to those obtained via the one-dimensional calculations. From figure 2(a) and (b) it can be seen that the 70 point non-uniform mesh, the eventual fully-developed particle concentration and velocity profiles are very similar to those obtained from the one-dimensional calculations. Hence, a maximum of 70 grid points in our non-uniform mesh was deemed satisfactory in order to produce sufficiently accurate simulations, such as those illustrated in figure 2(a) and (b).

Figure 3(a) and (b) show the particle concentration and velocity profiles, respectively, when the problem is solved with λ kept constant at 0.05 but with β increased to 150, with $\hat{u} = \frac{1}{6}$ and $\phi_s = \frac{3}{20}$. An obvious difference caused by increasing β is that the particle concentration within the bottom region of the channel decreases, as seen by comparing figures 2(a) and 3(a). When the flow becomes fully-developed the particle concentration on the bottom surface is about 0.43 when $\beta = 150$ compared to 0.47 when $\beta = 50$. As β increases the ratio between the characteristic flow velocity, U_0, and the Stokes settling velocity, u_t, increases but since the particle flux, see [65], is assumed unchanged then u_t must decrease. Thus, since u_t decreases as β increases, then the rate of the particle settling decreases and hence the particle concentration near to the bottom surface of the channel decreases. Additionally, by comparing figures 2(b) and 3(b), it can be seen that the u-component of the velocity within the suspension region is greater in the case $\beta = 150$ than in the case $\beta = 50$. However, the maximum u-component of velocity, which occurs just outside the suspension region, is greater in the latter case. These observations are compatible with the particle concentration profiles shown in figures 2(a) and 3(a), i.e. the effective viscosity, see [4], within the suspension region for $\beta = 150$ is less than that for $\beta = 50$. Thus, the suspension layer in the former case flows more easily than in the latter case. However, since the flux of clear fluid across the channel remains constant, the magnitude of this flux within the clear fluid region must be greater in the case $\beta = 50$, i.e. the maximum u-component of velocity is larger when $\beta = 50$.

Figure 4(a) and (b) show the particle concentration and velocity profiles, respectively, when the problem is solved with β kept constant at 50 but with λ increased to 0.1, with $\hat{u} = \frac{1}{6}$ and $\phi_s = \frac{3}{20}$. By increasing λ it is observed from figures 2(a) and 4(a), that the particle concentration within the suspension layer has decreased. If the channel height is unchanged then by increasing λ, i.e. the ratio between the particle radii and the channel height, we are effectively increasing the particle radii. Physically, spheres are more likely to interact with one another if their spatial size is greater, i.e. small spheres within a stratified shear flow are more likely to slip past each other than larger spheres. Thus, the shear-induced diffusive flux increases as λ increases, since there are more particle interactions occurring, and hence the amount of migration from regions of high concentration to regions of lower concentration also increases, as illustrated by comparing figure 2(a) with 4(a). Conversely, if λ decreases then it is expected that the corresponding diffusive flux reduces and hence a more concentrated suspension layer is likely to form. This is illustrated in figure 5(a) and (b), which show the particle concentration and velocity profiles, respectively, when the problem is solved with β kept constant at 50 but with λ decreased to 0.005 and the values of $\hat{u}$ and ϕ_s are unchanged. By decreasing λ a thick stagnant sediment layer of maximum particle concentration forms on the lower surface of the channel in the immediate vicinity of the entrance. However, the rate of depletion of the particles from the upper region of the channel was less than that observed when $\lambda = 0.05$. This is because, even at small values of x, the suspension in the region just above the lower surface of the channel becomes stagnant and if the particle and clear fluid fluxes are to be conserved their contributions from within the rest of the suspension, i.e. not including the stagnant region, must increase. This results in the u-component of the bulk velocity increasing away from the stagnant region, see figure 5(b), and thus the shear flow builds up rapidly which in itself induces a diffusive flux that opposes sedimentation. For the case $\lambda = 0.05$, the shear within the suspension layer begins to increase at a greater distance along the channel than compared to the current case. For this reason the sedimentation flux is counteracted at a much shorter distance along the channel when $\lambda = 0.005$ compared to that when $\lambda = 0.05$. Thus, when $\lambda = 0.05$ the

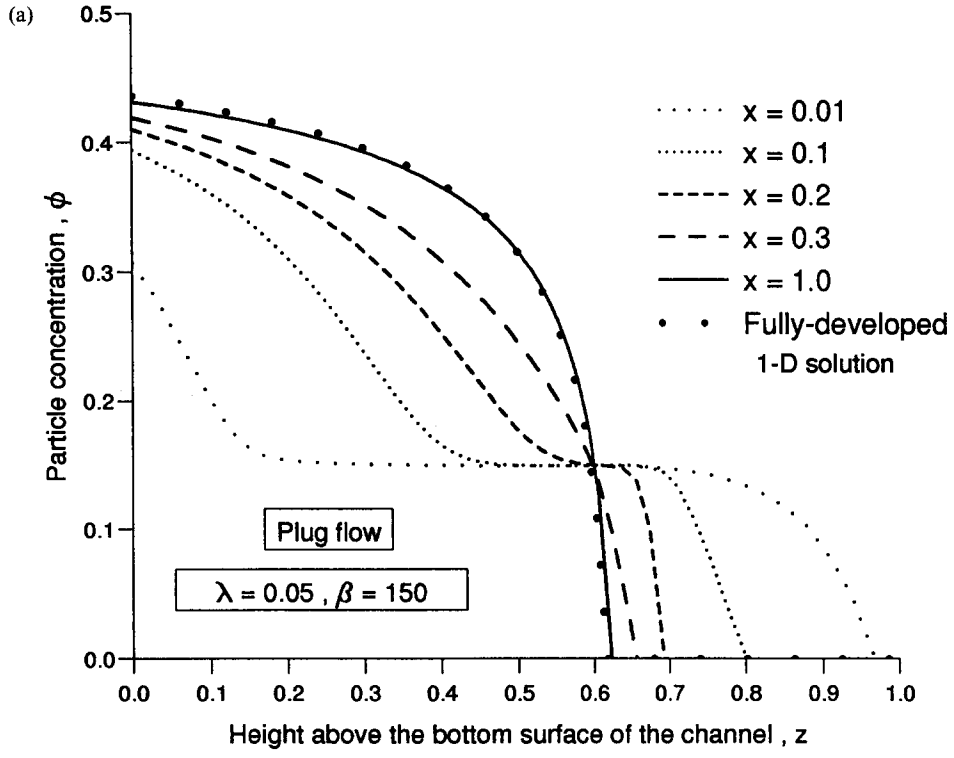

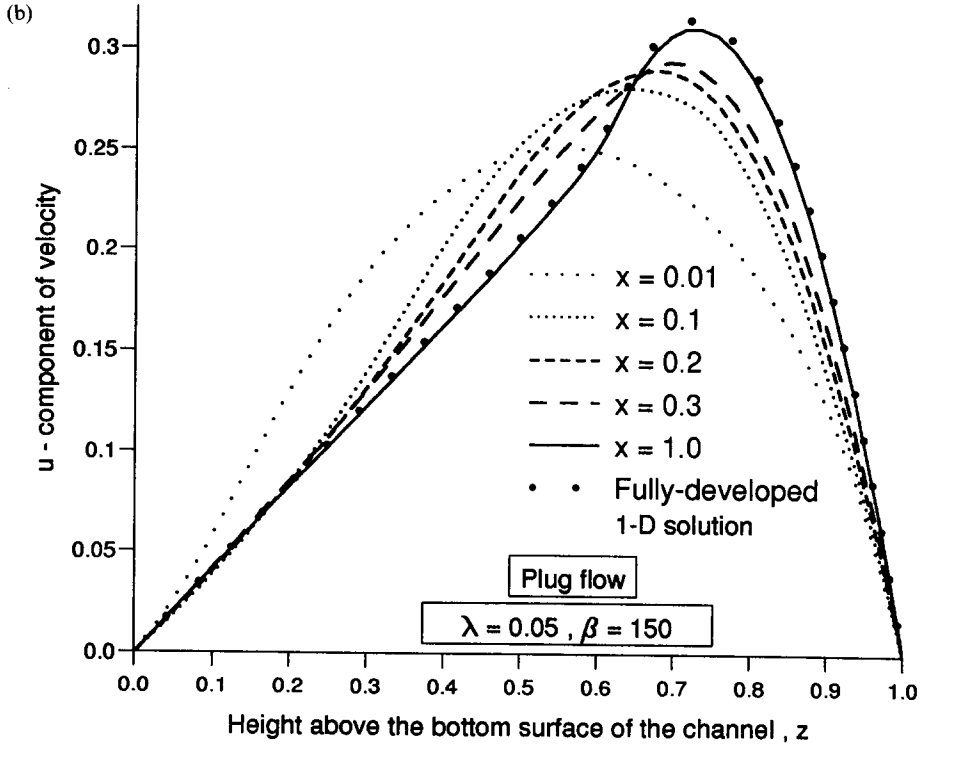

Figure 3. (a) The variation of the particle concentration, ϕ, with the height above the bottom surface of the channel, z, for an initial plug of well-mixed suspension of particle concentration 0.15 with $\mathrm{Rp} = 10^{-3}$, $\epsilon = 1$, $\lambda = 0.05$ and $\beta = 150$ flowing along a horizontal channel. (b) The variation of the u-component of velocity with the height above the bottom surface of the channel, z, with conditions as in (a).

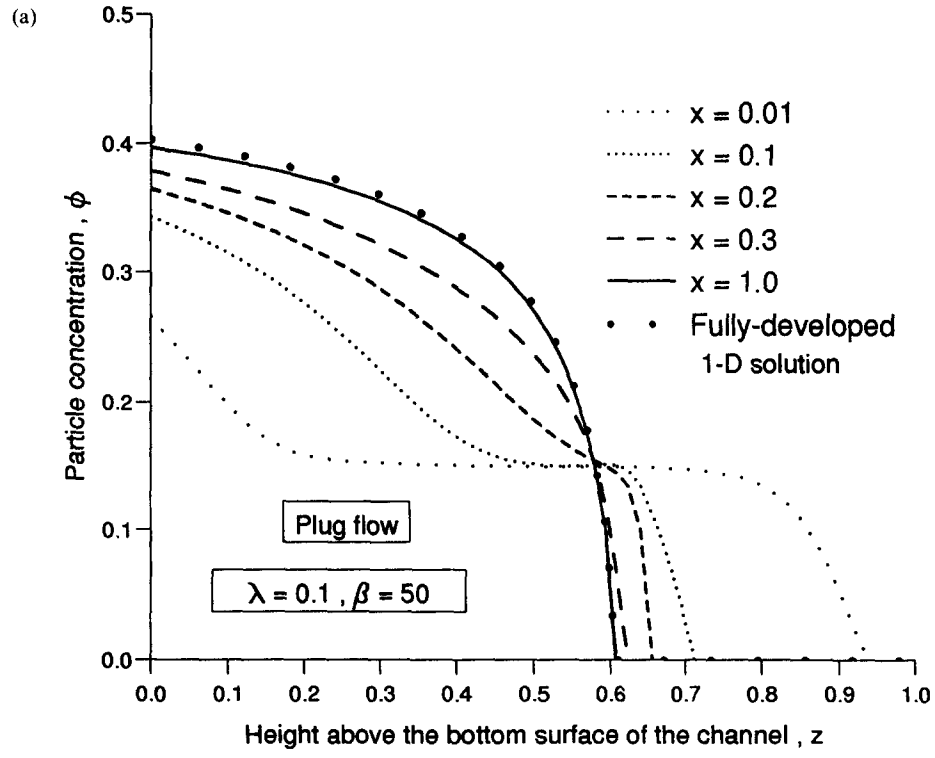

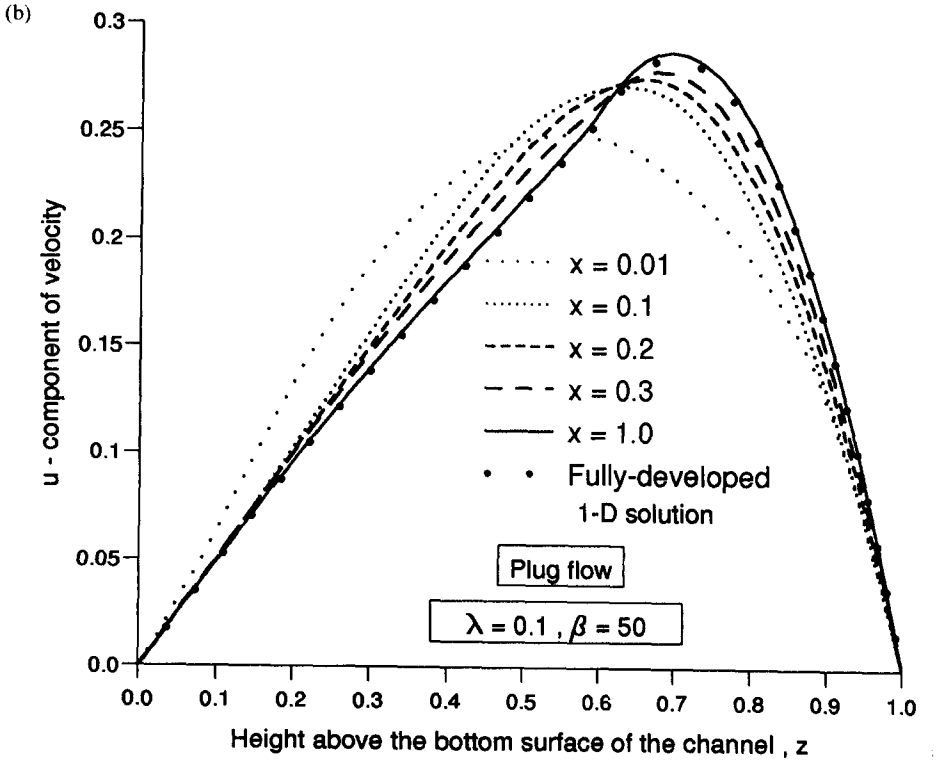

Figure 4. (a) The variation of the particle concentration, ϕ, with the height above the bottom surface of the channel, z, for an initial plug of well-mixed suspension of particle concentration 0.15 with $Rp = 10^{-3}$, $\epsilon = 1$, $\lambda = 0.1$ and $\beta = 50$ flowing along a horizontal channel. (b) The variation of the u-component of velocity with the height above the bottom surface of the channel, z, with conditions as in (a).

suspension layer depletes so that the suspension-clear fluid interface drops to just above $z = 0.6$, compared to $z = 0.8$ when $\lambda = 0.005$. Figure 5(c) and (d) illustrate the particle concentration and velocity profiles, respectively, when the problem is solved with λ held constant at 0.005, but with β increased to 1000, and the values of $\hat{u}$ and ϕ_s unchanged. By increasing β to 1000 it can be seen, on comparison with figure 5(a) and (c), that the particle concentration profiles evolve in a similar manner to those observed for $\beta = 50$, except in this case the concentration on the bottom surface is lower. In this case the particle concentration on the bottom surface of the channel is 0.54 when the flow becomes fully-developed, compared to 0.58 when $\beta = 50$. Additionally, on comparing figure 5(b) and (d), it can also be seen that the u-component of the velocity with the suspension is greater when $\beta = 1000$ than when $\beta = 50$, but the opposite is true just outside the suspension region. Explanations for these observations were discussed earlier in this section.

In the study undertaken by Pelekasis & Acrivos (1995), the steady laminar flow of a well-mixed suspension of monodisperse solid spheres, convected steadily past a horizontal flat plate and sedimenting under the action of gravity, was examined. In that problem the particle concentration profile was found to be non-uniform within two regions either side of the flat plate. This was due to the presence of shear-induced particle diffusion that balanced the particle flux due to convection and sedimentation. In this study so far it is only possible to compare the value of the particle concentration at the top surface of the plate in the work of Pelekasis & Acrivos (1995) to that at the bottom surface of the horizontal channel. This is because, although sedimentation is the dominant process affecting the particle concentration on both the bottom side of the plate and the top surface of the channel, the particle concentration is always zero on the top surface of the channel due to the initial entrance profile used so far. It is shown later, when a uniform plug of well-mixed suspension enters the channel, that the depletion of particles from the top surface of the channel is similar to that on the bottom of the plate considered by Pelekasis & Acrivos (1995), i.e. the particle concentration in both cases tends to zero at small values of x. On the other hand, figure 6 shows how the particle concentration on the bottom surface of the channel varies with the distance along the channel, x, obtained for various values of λ when $\beta = 50$ and 150. It is observed that the particle concentration on the bottom surface of the channel decreases if either λ or β are increased. Also, it is clear from these profiles that the particle concentration on the bottom surface initially increases fairly rapidly with respect to x but eventually levels off and becomes almost constant. This is quite different to the profiles obtained in Pelekasis & Acrivos (1995), where the particle concentration continually increases with x up to the maximum packing concentration, $\phi_0 = 0.58$. Intially, the increase in concentration with respect to x, as predicted by Pelekasis & Acrivos (1995), is quite rapid as in our case but then the rate of increase slows and becomes approximately constant until it rapidly increases when maximum packing is approached. The reason for this is that Pelekasis & Acrivos (1995) have considered a Blasius type solution in which the shear stress remains constant within the diffusion layer unlike that observed in our problem. Consequently, as the sedimentation above the plate increases a region of increasing viscosity together with its inversely proportional shear rates is formed, which in turn reduces the diffusive flux opposing sedimentation. The reason for the sharp increase in ϕ with respect to x as maximum packing is approached is a result of the rapid increase of the viscosity in this situation, i.e. $\mu_r \to \infty$ as $\phi \to \phi_0$. For small values of λ, e.g. $\lambda = 0.005$, the particle concentration on the bottom surface achieves the constant maximum packing value close to the entrance into the channel. This is because for such cases sedimentation effects dominate those due to shear-induced diffusion. The contribution of the particle flux due to shear rate gradients, which is neglected in this study, would serve to counteract sedimentation effects and thus avoid the immediate occurrence of the maximum particle packing on the bottom surface channel.

For the values of $\hat{u}$ and ϕ_s adopted in the results presented in figures 2–5, the non-dimensional development length proposed by Schaflinger *et al.* (1995), and expressed by [33], is such that $L_\phi/H \sim 17\beta/960$. A quantitative comparison between the experimental and numerical results is difficult for a variety of reasons. However, a qualitative comparison suggests

(i) in the experiments with $\phi_s \ll 1$ and $\beta \gg 1$ the value of $L_\phi/H \ll 5$, whilst the velocity and concentration profiles indicate that the fully developed situation has been reached, or is very close to being reached, before L_ϕ/H reaches unity.

(ii) the figures 5(b) and (d) clearly show that when $\beta = 50$ the maximum velocity is within about 10% of its fully developed magnitude at $x = 0.1$, whilst at the same position when $\beta = 1000$ the maximum velocity is only within about 25% of its fully developed magnitude. This indicates an increase in the magnitude of L_ϕ/H with increasing β. However, the fact that the results presented

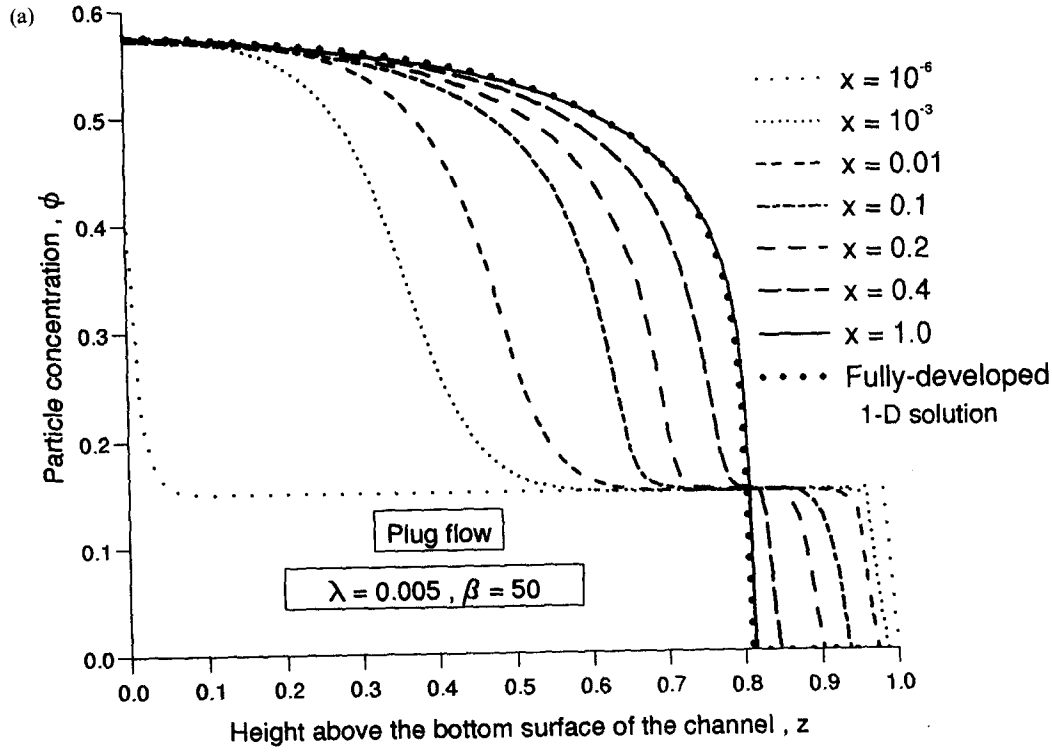

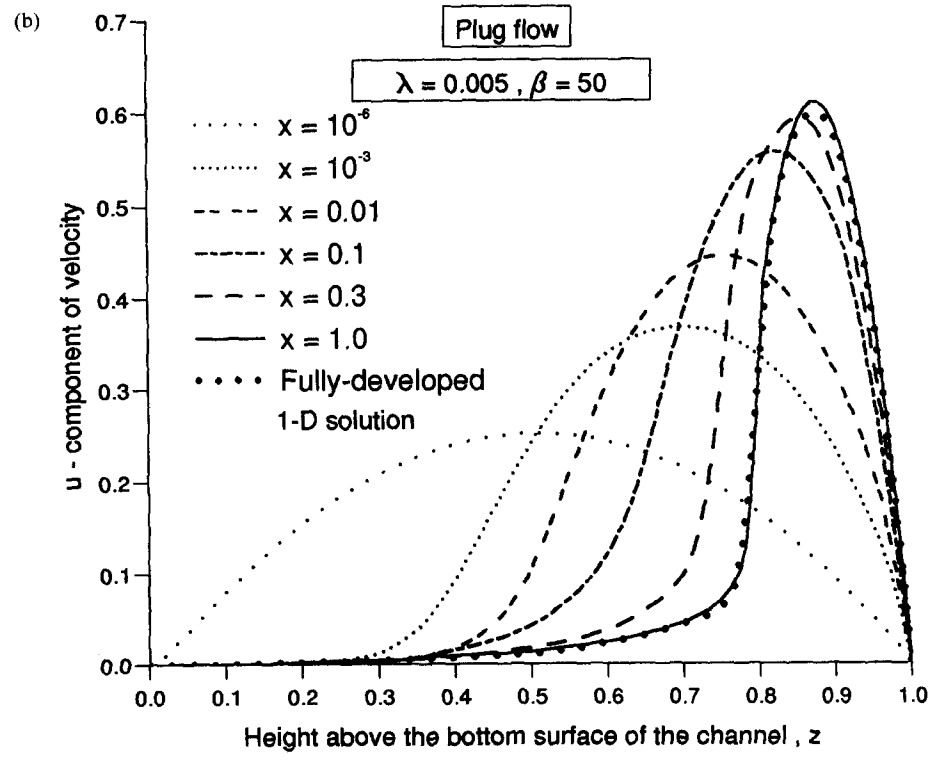

Fig. 5(a) and (b)

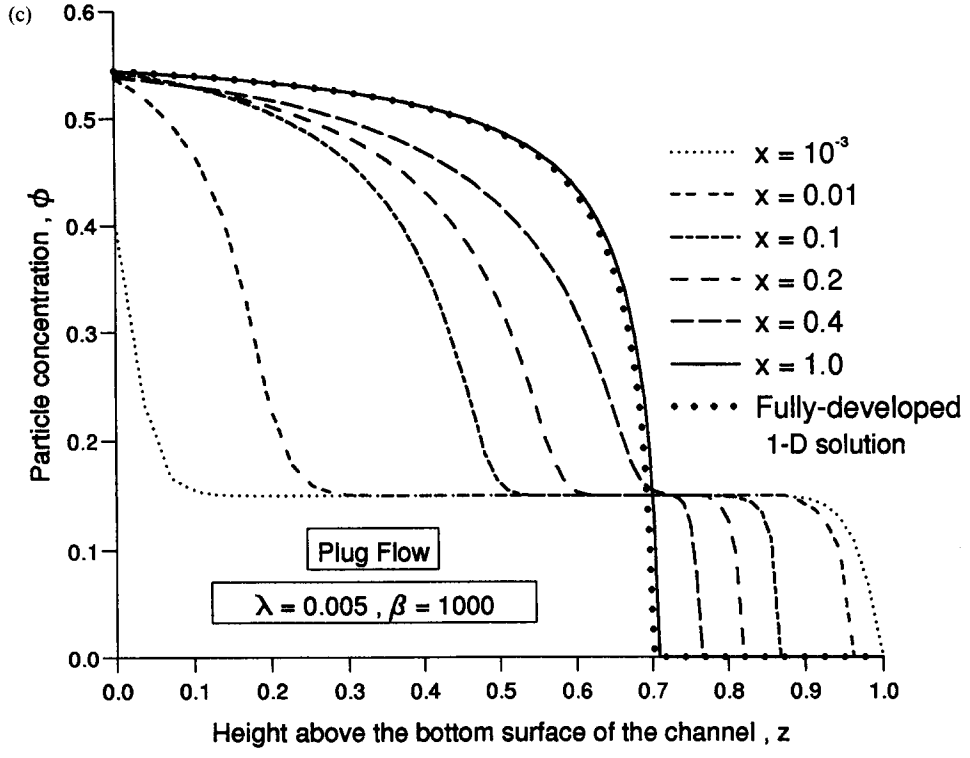

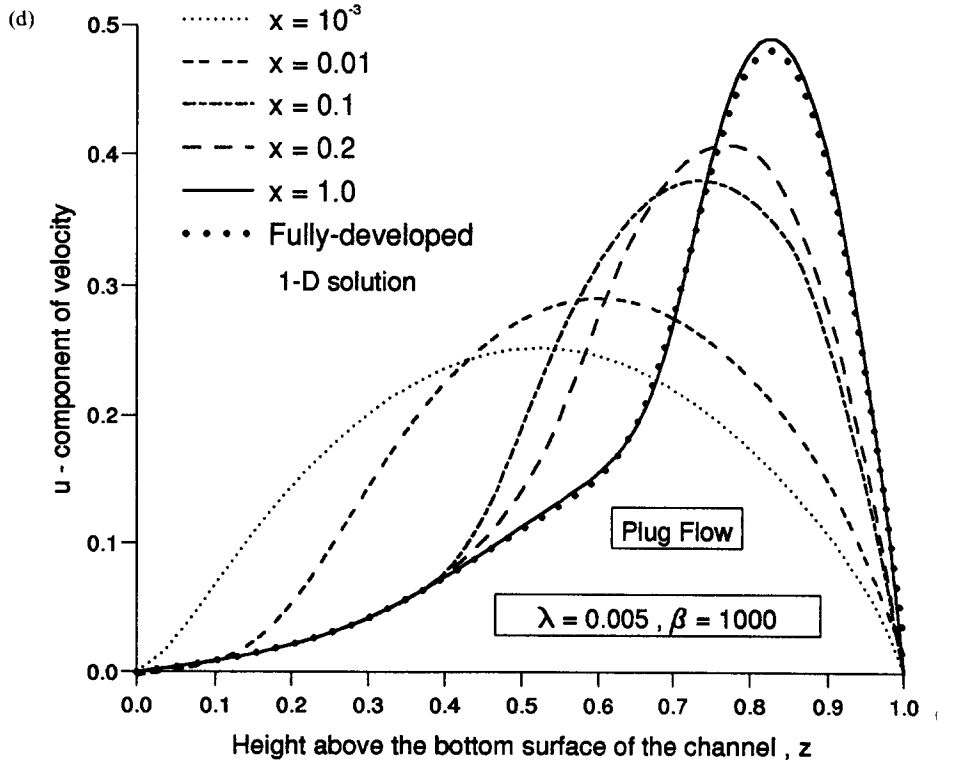

Figure 5. (a) The variation of the particle concentration, ϕ, with the height above the bottom surface of the channel, z, for an initial plug of well-mixed suspension of particle concentration 0.15 with Rp = 10^{-3}, $\epsilon = 1$, $\lambda = 0.005$ and $\beta = 50$ flowing along a horizontal channel. (b)The variation of the u-component of velocity with the height above the bottom surface of the channel, z, with conditions as in (a). (c) The variation of the particle concentration, ϕ, with the height above the bottom surface of the channel, z, for an initial plug of well-mixed suspension of particle concentration 0.15 with Rp = 10^{-3}, $\epsilon = 1$, $\lambda = 0.005$ and $\beta = 1000$ flowing along a horizontal channel. (d) The variation of the u-component of velocity with the height above the bottom surface of the channel, z, with conditions as in (c).

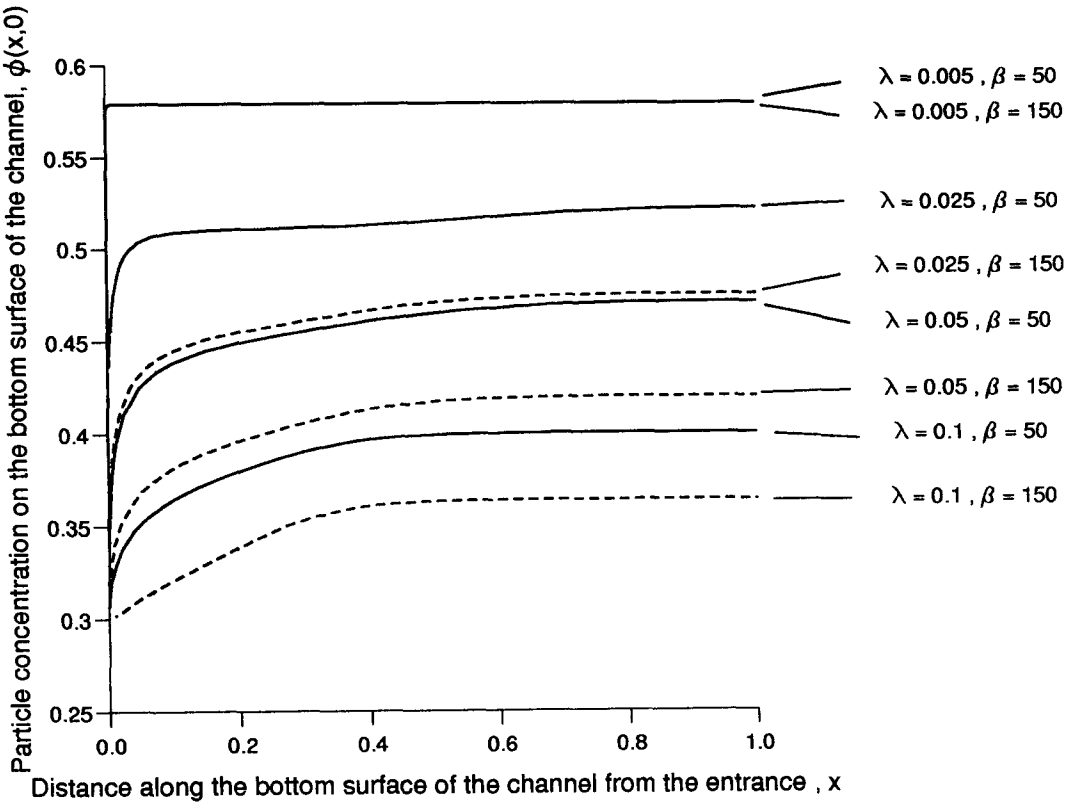

Figure 6. The variation of the particle concentration, ϕ, on the bottom surface of the horizontal channel with the distance along the channel, x, for an initially well-mixed plug of suspension of particle concentration 0.15 with $\mathrm{Rp} = 10^{-3}$, $\epsilon = 1$ for various values of λ and β.

in figure 5(d) indicate that L_ϕ/H does not exceed unity, even when $\beta = 1000$, whereas the non-dimensional development length expression proposed by Schaflinger *et al.* (1995) suggests $L_\phi/H \sim 17$, indicating that a small coefficient is required for equality in [33]. A fact supported by the experiments, where $L_\phi/H \ll 5$ thoughout.

When the channel is inclined at an angle α (>0) to the horizontal, then the pressure gradient $\partial p/\partial x$ drives the fluid together with the gravitational pressure gradient component, $-9\phi \sin\alpha/(2\lambda\beta\mathrm{Rp})$. If free flow conditions are to be achieved when the flow becomes fully-developed we must find β, via [31], which corresponds to the appropriate value of κ obtained in the one-dimensional calculations, see [30], when $K = -9\phi \sin\alpha/(2\epsilon\lambda\beta\mathrm{Rp})$ where ϵ is defined by [3] and it is taken to be unity in our calculations. If free flow conditions are to prevail when the flow becomes fully-developed then the pressure gradient, $\partial p/\partial x$, must tend to a constant vlaue, namely, $-9\phi \sin\alpha/(2\epsilon\lambda\beta\mathrm{Rp})$. Figure 7(a) and (b) show the particle concentration and velocity profiles, respectively, for the situation when a well-mixed plug of suspension enters the two-dimensional channel which is inclined at 15° to the horizontal with the parameters λ and β set as 0.05 and 26, respectively, with $\hat{u} = \frac{1}{6}$ and $\phi_s = \frac{3}{20}$. As for the plug flow in the horizontal channel the initial particle concentration and velocity profiles are $\phi_s(z) = \frac{3}{20}$ and $\hat{u} = \frac{1}{6}$, respectively. The qualitative nature of the profiles obtained is very similar to the behaviour seen for the horizontal channel. In addition, the eventual fully-developed particle concentration and velocity profiles, see figures 7(a) and (b), respectively, are in good agreement to those corresponding profiles which were obtained by solving the fully-developed one-dimensional gravity-driven flow calculations, see [29] and [30]. When the angle of inclination increases to 30°, with the entrance conditions remaining unchanged, we require $\beta = 150$ for eventual free flow in the fully-developed situation. Again, our results agree well with those obtained via the one-dimensional calculations, see figure 8(a) and (b) which show the particle concentration and velocity profiles, respectively. It should be noted that the parameter values $\lambda = 0.05$ and $\beta = 150$ were also used in a corresponding horizontal channel

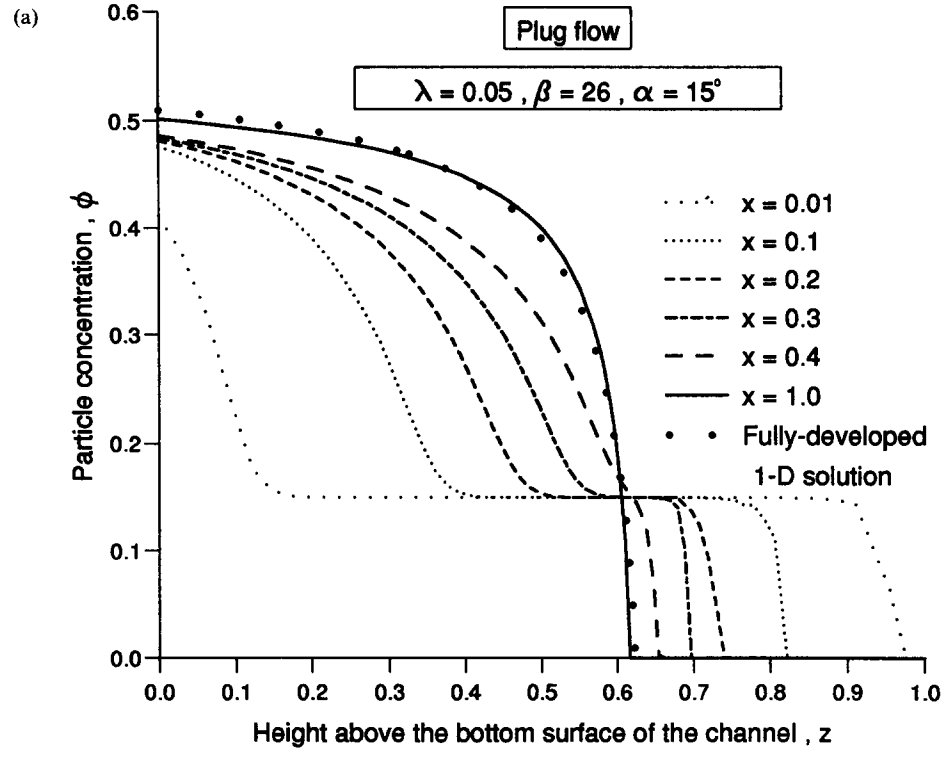

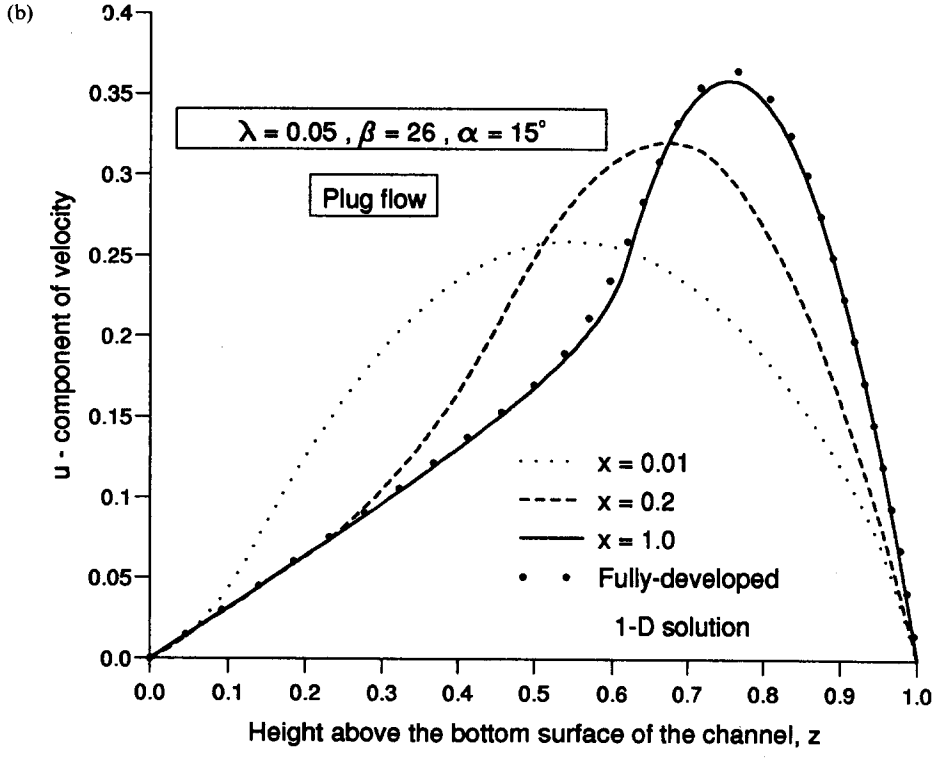

Figure 7. (a) The variation of the particle concentration, ϕ, with the height above the bottom surface of the channel, z, for an initially well-mixed plug of suspension of particle concentration 0.15 with $\mathrm{Rp} = 10^{-3}$, $\epsilon = 1$, $\lambda = 0.05$ and $\beta = 26$ flowing down a channel inclined at an angle 15° to the horizontal. (b) The variation of the u-component of velocity with the height above the bottom surface of the channel, z, with conditions as in (a).

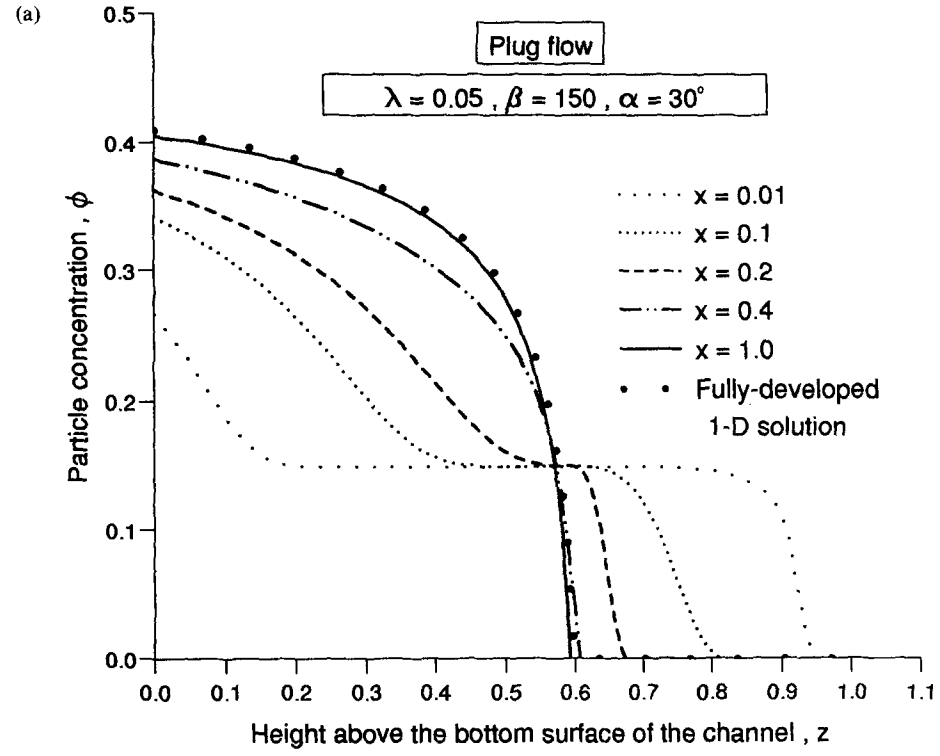

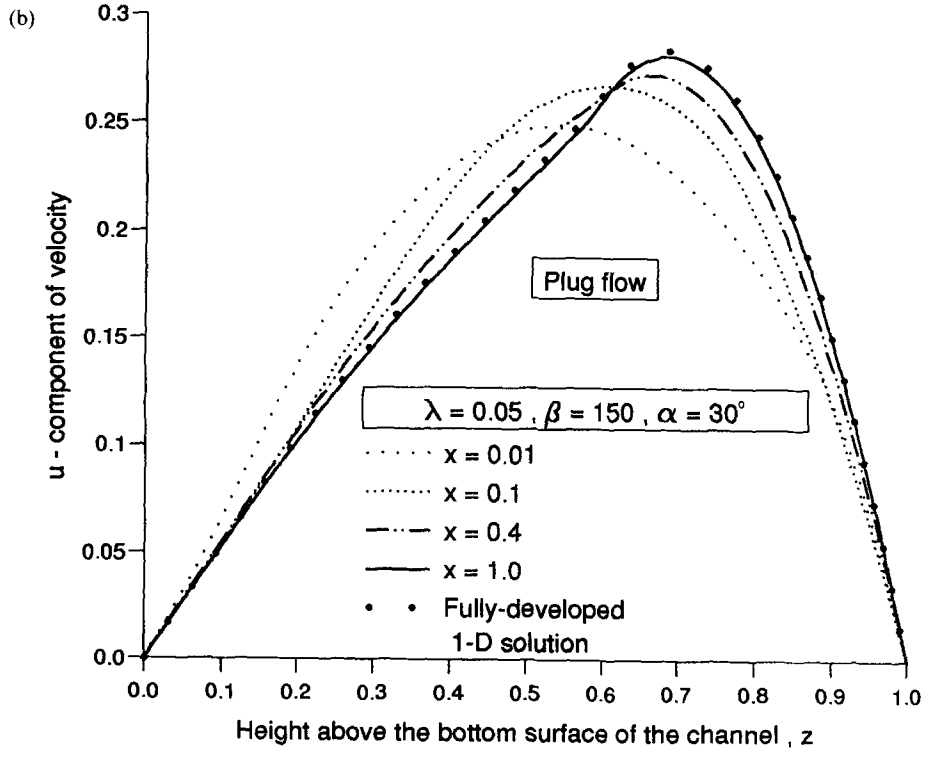

Figure 8. (a) The variation of the particle concentration, ϕ, with the height above the bottom surface of the channel, z, for an initially well-mixed plug of suspension of particle concentration 0.15 with $Rp = 10^{-3}$, $\epsilon = 1$, $\lambda = 0.05$ and $\beta = 150$ flowing down a channel inclined at an angle of 30° to the horizontal. (b) The variation of the u-component of velocity with the height above the bottom surface of the channel, z, with conditions as in (b).

flow. The only noticeable difference in the two cases can be highlighted by comparing figures 3(a) and 8(a). It is observed that the particle concentration on the bottom surface of the channel is 0.42 in the horizontal situation, compared to about 0.40 in the inclined situation. This result could be attributed to the fact that in the inclined situation the particle flux due to sedimentation is proportional to $\cos \alpha$ and hence its magnitude decreases as α increases.

5. CONCLUSIONS

In this study the problem of a uniform particulate suspension entering a channel with a uniform velocity profile has been examined. The parabolic system of partial differential equations governing the flow were discretised using finite differences and a marching procedure, aided by a Newton–Raphson iterative method, was used to obtain their solution. In order to check the accuracy of the numerical scheme devised the following tests were used:

(i) The particle flux must remain constant.

(ii) The eventual fully-developed flow profiles must agree with the corresponding profiles obtained by solving the governing system ordinary differential equations which result when there is no x-dependence.

When a uniform mesh was used across the channel the accuracy of the solutions obtained was not satisfactory. To increase the accuracy of the solutions and to maintain numerical stability a non-uniform mesh system was used in which more finite-difference grid points have to be assigned in the region of the eventual suspension-clear fluid interface. By using such a technique, the percentage error in the particle flux decreased to less than unity and the eventual fully-developed solutions matched the corresponding one-dimensional solutions.

Initially, the suspension was assumed to enter a horizontal channel and the parameter λ was varied through a realistic range of experimental values appropriate to the flows of proppant in hydraulic fractures, while β was kept unchanged. It was found that the flow was very strongly influenced by λ. In particular, at small values of λ, the particle concentration within the suspension layer began to approach the maximum packing value and the thickness of this layer increase so as to cover almost the entire channel. This resulted in the formation of a thick, stagnant suspension layer above which a narrow layer of rapidly flowing clear fluid existed. As λ increases the height of the suspension layer decreases, as does the particle concentration within it. Additionally, an increase in λ results in an increase in the u-component of velocity within the suspension layer but a decrease in the strong flow in the clear fluid layer. When β was varied and λ kept constant the flow was again influenced but not as strongly as that in the previous case when λ was varied with β constant. It was found that as β increases the particle concentration above the bottom surface of the channel began to decrease, and vice versa, but the thickness of the suspension layer was virtually unaffected. In all the simulations the initially uniform velocity profiles almost instantaneously became parabolic at the entrance of the channel. However, the corresponding particle concentration profiles developed less dramatically with sedimentation effects dominating at small values of x, but which were counteracted by shear-induced diffusive effects at larger values of x. It is found that the particle concentration increases above the bottom surface of the channel and depletes from below the upper surface and the rate of increase or depletion depends on the parameter λ. When λ is small the particle concentration builds up to the maximum packing value above the bottom surface of the channel at small values of x but the rate of depletion from below the top surface is slow. At larger values of λ although the increase in particle concentration above the bottom surface is more gradual the decrease from below the top layer is much more rapid and gives rise to the formation of a substantial clear fluid layer even at small values of x. In the region where the eventual suspension-clear fluid interface is located when the flow becomes fully-developed the particle concentration remains at its initial uniform entrance value for a considerable distance down the channel. It is found that the particle concentration increases below this region and decreases above it. However, the width of this region of constant concentration continues to decrease as one moves further down the channel. Eventually, when the flow becomes fully-developed, this region of uniform particle concentration disappears.

When the channel is inclined at an angle α to the horizontal, the parameters λ and β were chosen so that the eventual fully-developed suspension flow would become solely gravity-driven. This was achieved by obtaining the values of the modified Shields number, κ, from the one-dimensional calculations and then calculating β via [31], provided λ was constant. With these combinations of parameters the initial plug of well-mixed suspension eventually develops into a purely gravity-driven flow. It was observed that the particle concentration within the suspension layer decreases as the angle of inclination of the channel increases. However, it was found that the qualitative behaviour of the suspension and the flow was very similar to that observed when pressure-driven flows were considered.

REFERENCES

Leighton, D. & Acrivos, A. 1986 Viscous Resuspension. *Chem. Engng. Sci.* **41,** 1377–1384.

Leighton, D. & Acrivos, A. 1987 The shear-induced migration of particles in concentrated suspensions. *J. Fluid Mech.* **181,** 415–439.

Pelekasis, N. A. & Acrivos, A. 1995 Forced convection and sedimentation past a flat plate *J. Fluid Mech.* **294,** 301–321.

Phillips, R. J., Armstrong, R. C., Brown, R. A., Graham, A. L. & Abbott, J. R. 1992 A constitutive equation for concentrated suspensions that accounts for shear-induced particle migration. *Phys. Fluids A* **4,** 30–40.

Powell, M. J. D. 1970 A hybrid method for nonlinear algebraic equations. In *Numerical Methods for Nonlinear Algebraic Equations* (Edited by Rabinowitz, P.).

Schaflinger, U., Acrivos, A. & Zhang, K. 1990 Viscous resuspension of a sediment within a laminar and stratified flow. *Int. J. Multiphase Flow* **16,** 567–578.

Schaflinger, U., Acrivos, A. & Stibi, H. 1995 An experimental study of viscous resuspension in a pressure-driven plane channel flow. *Int. J. Multiphase Flow* **21,** 693–704.

Yilmazer, U. & Kalyon, D. M. 1989 Slip effects in capillary and parallel disk torsional flows of highly filled suspension. *J. Rheol.* **33,** 1197–1212.

Zhang, K. & Acrivos, A. 1994 Viscous resuspension in fully developed laminar pipe flows. *Int. J. Multiphase Flow* **20,** 579–591.